On the Design of SC Walls for Missile Impact: Summary of Tests and Simulations

Joo Min Kim[a*], Amit Varma[b]
[a]*Principal Researcher, Korea Atomic Energy Research Institute, Daejeon, South Korea.*
[b]*Professor, School of Civil Engineering, Purdue University, West Lafayette, IN 47907, United States.*
[*]*Corresponding author: joominkim@kaeri.re.kr*

1. Introduction

Reinforced concrete (RC) structures are commonly used as protective structures. Methods to design RC walls against missile impact are well established and validated theoretically and experimentally for decades. Steel-plate composite (SC) walls are growing in popularity as an alternative to RC walls due to advantages such as efficiency in construction and excellent structural performance. SC structures are currently used in containment internal structures (CIS) of pressurized water reactors (PWRs) and are being considered for use in small modular reactors (SMRs).

SC walls are comprised of two steel faceplates, steel-headed shear stud anchors, tie bars, and concrete infill. Steel faceplates create exterior boundaries to serve as formwork during construction. These same faceplates provide flexural reinforcement for the wall. Steel-headed shear stud anchors are welded to the inner surface of steel faceplates and embedded in the concrete to bond the steel faceplates and the concrete infill. Tie bars provide stability to the walls during erection and maintain the wall thickness by connecting the two exterior steel faceplates.

Impactive design of SC wall structures is an important topic in safety-related nuclear facilities. Bruhl et al. (2015) proposed a three-step design method of SC walls against impact load, specifically to design SC walls to prevent perforation by projectiles. While the method was validated using the existing database of tests, it has not been specifically evaluated and validated by an experimental program designed to confirm its accuracy.

This paper presents a summary of experimental and analytical research conducted to study local failure behavior of SC walls subjected to missile impact. Discussion of SC wall specimen design, test setup, and tests results are provided. Test data such as perforation check (whether or not the projectile was stopped by or perforated the wall), penetration depth, and bulging depth were examined. Numerical models were developed to simulate the experimental tests and estimate an extent of damage on the SC wall specimens. Local failure behavior in the numerical models was investigated and were benchmarked with the experimental test data.

2. Experimental program

2.1 Specimen Design and Details

This experimental program investigated the behavior of five different SC wall designs. These designs varied flexural reinforcement ratio ($\rho = 2tp/tsc$), shear reinforcement ratio ($\rho t = Atie/S2$), and steel faceplate yield strength (fy). Among the specimens, flexural reinforcement ratio varied from 3.7% to 5.2%, shear reinforcement ratio varied in the range between 0.37% to 1.23%, and faceplate nominal yield strength varied from 50 ksi to 65 ksi. All of them have the same global dimensions as 4 in. × 16 in. × 11 in. The three-dimensional rendering image and SC module before concrete cast were illustrated in Figure 1. These images illustrate the location and spacing of tie bars and stud anchors.

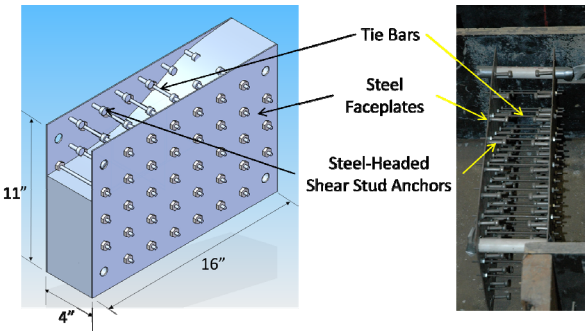

Figure 1 Three-dimensional rendering and module of SC wall specimen (Kim et al. 2017b)

The steel faceplates were comprised of A1011 steel sheet. Two different strength plates (Gr50 and Gr65) and two thicknesses (gage 12 and gage 14) were used – material properties are provided in Table 1. Steel-headed shear stud anchors (or shear studs) which were 1.125 in. long with 0.25 in. diameter were welded to interior surface of the steel faceplates. Threaded rods were used as tie bars and secured with hex nuts on top and bottom of each steel faceplate. Normal weight concrete with pea-gravel was used for concrete infill of SC wall specimens with the maximum aggregate size of 3/8 in. diameter. Design compressive strength of the concrete was 5 ksi. Actual compressive strength was measured at the day of each test. These SC wall specimens design referred to AISC N690s1-15, Appendix N9 (AISC 2015). Pertinent design parameters of the SC wall specimens are summarized in Table 1.

Projectiles were cut from AISI 4340 round stock and heat treated to provide a minimum 42-45 C Rockwell hardness. Their material properties were 194 ksi yield

strength and 206 ksi ultimate strength by coupon tests. Sabots were manufactured from polypropylene; its compressive strength was 4.8 ksi.

Table 1 Design details of the SC wall specimens

Specimen identifier	t_{sc} (in)	t_p (in)	ρ (%)	s/t_p	d_s/t_p	S/t_{sc}	ρ_t (%)	f'_c (ksi)	f_y^{pl} (ksi)	s (in)	d_s (in)	S (in)	d_t (in)
3.7-0.37-50	4	0.0747	3.7%	26.8	3.3	0.5	0.37%	6.52	56	2	0.25	2	0.1380
3.7-0.37-65	4	0.0747	3.7%	26.8	3.3	0.5	0.37%	5.94	73	2	0.25	2	0.1380
3.7-0.53-50	4	0.0747	3.7%	26.8	3.3	0.5	0.53%	6.38	56	2	0.25	2	0.1640
5.2-0.48-50	4	0.1046	5.2%	19.1	2.4	1.0	0.48%	6.53	58	2	0.25	4	0.3125
3.7-1.23-50	4	0.0747	3.7%	26.8	3.3	0.5	1.23%	6.18	56	2	0.25	2	0.2500

2.2 Test Setup and Instrumentation

Total of 16 tests were conducted in the Robert L. and Terry L. Bowen Laboratory in Lyles School of Civil Engineering, Purdue University. Figure 2 shows the photograph of the installed test setup. Pressurized nitrogen launched the projectiles through a 2.5 in. diameter gun barrel. Projectiles were inserted into a specially-fabricated sabot to maintain a seal between the gun barrel and the sabot and help ensure level flight of the projectile exiting the barrel.

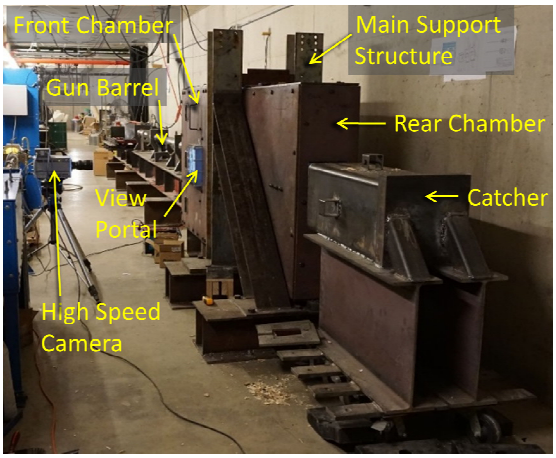

Figure 2 Photograph of test setup (Kim et al. 2017a)

The SC wall specimen was fixed to the main support structure which was anchored to the floor. Impact of the projectile onto the SC wall specimen occurred within the front chamber which confined any shrapnel caused by the impact. The rear chamber collected the projectile and debris of the SC wall specimen for those the projectiles which perforated the specimen. The "catcher" was the final chamber to collect anything that passed through the rear chamber.

A high-speed camera recorded the impact on the front faceplate through a view portal on the front chamber. The view portal was covered with 2 in. thick polycarbonate plate which is transparent and projectile resistant. Photron Fastcam APX PX model was used with parameters set accordingly to: frame rate of 14,000 fps, shutter speed of 1/61000 and resolution of 640 × 304 pixels. Figure 3 shows a representative recorded image which was taken immediately before impact. The projectile was moving forward to the specimen (from left to right in the image) and was contained by the sabot. A scaled checker board was placed in rear of the projectile for the measurement of travel distance of the projectile. A measuring device was attached on the upper part of checker board to increase accuracy of measurements using the high-speed video recordings. The SC wall specimen is on the right side of the image.

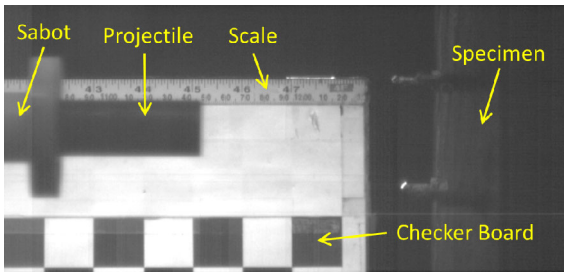

Figure 3 Captured image of inside of the front chamber by high speed camera (Kim et al. 2017b)

2.3 Experimental Tests Results

This paper reports results from ten representative tests excerpted from the entire set of tests (Kim et al. 2021) to benchmark numerical models developed in the following sections. For convenience, these tests are referred to by test number (1 through 10 as listed in Table 2). Details of the projectile (weight, diameter, and impact velocity) along with observed and measured damage of the SC wall specimen is summarized in Table 2. Reported damage includes perforation check, damage mode, impact velocity, penetration depth, and bulging depth. The test case identifier consists of six terms which describe specimen and projectile parameters. The first three terms indicate flexural reinforcement ratio, shear reinforcement ratio and steel faceplate yield strength of the SC wall specimen. In the presented test cases, the reinforcement ratio was limited to 3.7% and the shear reinforcement ratio varied in the range between 0.37% and 1.23%. The yield strength of the steel faceplates was limited to 50 ksi. The next three terms in the test identification indicate the diameter, weight, and target velocity of the projectile. Flat-nosed projectiles with 1.0 in. and 1.5 in. diameter were used and their weight varied in the test cases: two different weights (1.3 lbs and 2.0 lbs) for 1.0 in. diameter projectile and three different weights (1.3 lbs, 2.0 lbs and 3.5 lbs) for 1.5 in. diameter projectile were applied. Actual projectile weight was measured for every test and included in the table. Impact velocity of the projectile was calculated using data from high-speed camera.

Table 2 Summary of experimental tests results

Test No.	*Test case identifier*	Projectile			*Test result*	*Damage mode*	*Penetration depth (in)*	*Rear faceplate bulging (in)*
		Weight (lb)	*Diameter (Nominal, in)*	*V_{imp} (ft/s)*				
1	3.7-0.37-50-1.0-1.3-554	1.316	1.0	593	Stopped	Bulging	2.06	0.25
2	3.7-0.37-50-1.0-1.3-677	1.301	1.0	674	Stopped	Bulging	3.06	0.63
3	3.7-0.37-50-1.0-2.0-430	1.991	1.0	424	Stopped	Bulging	1.56	0.25
4	3.7-0.37-50-1.0-2.0-525	2.000	1.0	513	Stopped	Bulging	3.16	0.58
5	3.7-0.53-50-1.5-1.3-660	1.303	1.5	667	Stopped	Bulging	1.38	0.56
6	3.7-0.53-50-1.5-1.3-750	1.301	1.5	760	Stopped	Bulging	2.00	0.72
7	3.7-0.53-50-1.0-2.0-513	2.000	1.0	640	Perforated	Perforation	-	-
8	3.7-0.53-50-1.0-2.0-626	1.991	1.0	710	Perforated	Perforation	-	-
9	3.7-1.23-50-1.5-3.5-380	3.521	1.5	550	Stopped	Splitting	4.00	1.63
10	3.7-1.23-50-1.5-3.5-465	3.541	1.5	489	Stopped	Bulging	1.91	0.59

After each test, the SC wall specimen was visually inspected. The extent of damage on the exterior surfaces such as cracks, penetration depth and bulging depth was recorded qualitatively and quantitatively. Qualitatively, the damage mode of each post-tested specimen was classified as one of three types: bulging, splitting and perforation. Quantitatively, penetration depth of the projectile into the specimen and bulging depth of the rear steel faceplate were measured manually. Penetration depth was measured by subtracting the exposed portion of the projectile from its total initial length. This measurement assumes no deformation on the front surface of the projectile which was confirmed by removing the projectile from several specimens. Bulging depth was measured using a contour gage on the rear steel faceplate.

Test numbers 1 to 6 and 10 each stopped the projectile but resulted in considerable damage. The front faceplate was punched through leaving a hole similar in diameter to the projectile. The concrete infill was penetrated by the projectile. Because the rear steel faceplate was bulged, the damage mode with these features was classified as “bulging”.

In test number 9, projectile impact velocity was increased by 44.3% than the target velocity in an attempt to ensure perforation occurred and somewhat different aspect of damage on the specimen was shown. The rear steel faceplate resulted in splitting in the central area with severe bulging. Damage mode for this test case was classified as “splitting”. Figure 5 (a) provides a photograph of the splitting damage mode.

In test numbers 7 and 8, projectile impact velocity was increased by 24.8% and 13.4%, respectively, then the target velocity in an attempt to ensure perforation occurred. In these cases, the projectiles passed completely through the SC wall specimens and this damage mode was classified as “perforation”. Figure 6 (a) shows a photograph of the perforation damage mode.

3. NUMERICAL SIMULATION AND BENCHMARKING

3.1 Finite Element Modeling Approach

Finite element models were developed to more thoroughly investigate the failure behavior of SC walls subjected to impact load. This modeling approach referred to previous research by Bruhl et al. (2015), but some modifications were made. The models account for all components of the walls and the physical interaction among them. LS-DYNA, a commercial finite element analysis software, was used to develop three dimensional models of each specimen, projectile, and portions of the support structure in contact with the SC wall specimens. Figure 4 shows the developed finite element model for the impact test.

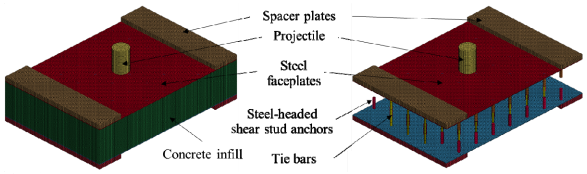

Figure 4 Finite element model developed in LS-DYNA (Kim et al. 2022)

The front and rear steel faceplates were modelled using solid elements with fully integrated and selectively reduced solid elements which are intended for elements with poor aspect ratios (ELFORM: -1). It uses eight integration points and reduces the shear locking phenomenon for poor aspect ratio elements. Piecewise linear plasticity (MAT_24) material type was adopted to represent material properties for the steel faceplates. Strain rate effect was considered in the finite element analysis using dynamic increase factor (DIF). UFC 3-340-02 (U.S. Department of Defense 2008) provides DIF values with regard to various strain rates for A514 plate. Although A514 plate is not exactly same material as A1011 steel sheet, its chemical composition is similar. So, the DIF values were used assuming they are applicable to A1011 steel sheet.

Tie bars and steel-headed shear stud anchors were modeled using beam elements with Hughes-Liu beam with cross section integration, which uses 2 x 2 Gauss quadrature rule (ELFORM: 1). The piecewise linear plasticity model (MAT_24) was used for tie bars and stud anchors to account for the non-linear plastic behavior of the steel material. Because the steel-headed shear stud anchors were simplified as one dimensional beam elements in the finite element model, the load-slip behavior (Ollgaard et al. 1971) caused by composite action was not inherently included. Therefore, a discrete beam element (ELFORM: 6) was added between the steel faceplates and the steel-headed shear stud anchors to account for the load-slip behavior of the steel-headed shear stud anchors.

The concrete infill was modeled using an eight-node constant stress solid element with single integration point (ELFORM: 1). Winfrith concrete with strain rate

effect included (MAT_84) was selected as the material type for the concrete infill.

The projectile was modeled using constant stress solid elements (ELFORM: 1) with material type of piecewise linear plasticity model (MAT_24). As an eight-node solid element, element formation of 1 element has a single integration point and needs hour glass stabilization. Belytschko-Bindeman hourglass type (TYPE 6) with hourglass coefficient setting to 0.1 (default) was used to control hourglass effects for the concrete infill and projectile elements.

Spacer plates were inserted on the top and bottom surfaces of the SC walls when they were fixed to the main support structure of the test setup. In the finite element model the spacer plates were modeled using constant stress solid elements (ELFORM: 1) and rigid material type (MAT_20) was used in order to reduce unnecessary analysis time; the structural behavior of these spacer plates was not of interest in this study. These spacer plates provided boundary conditions to the SC walls, which were implemented by constraint option.

AUTOMATIC_SURFACE_TO_SURFACE command with SOFT=0 was used to implement contact between front/rear steel plates and spacer plates, which is penalty-based contact approach. The same command with SOFT=1 was used for contact between steel plates and concrete infill where soft constraint-based contact approach was applied. ERODE_SURFACE_TO_SURFACE command with SOFT=1 and EROSOP=1 was chosen for contact among the projectile, front/rear steel plates, and concrete infill where element failure occurs and new contact faces are generated. AUTOMATIC_BEAM_TO_SURFACE command with SOFT=1 option was applied for contact between the projectile and tie bars and shear studs so that beam to solid contact works properly when the projectile penetrates SC walls. Steel-headed shear stud anchors and tie bars are embedded in the concrete core of SC walls. Perfect bond between these steel elements and the concrete core was assumed and implemented using command of CONSTRAINED_LAGRANGE_IN_SOLID.

3.2 Numerical Analyses Results and Benchmarking

The finite elements models were benchmarked using results from the experimental investigation. Table 3 shows the comparison of the results. Penetration depth of the projectile and bulging depth of the rear steel faceplate on the specimen measured after each test were compared with the numerical analyses results as a ratio (x_{c_FEM}/x_{c_test} and x_{bg_FEM}/x_{bg_test}, respectively). This ratio helps evaluate the accuracy of estimations that the numerical models provide. As was described for the experimental results, the damage mode from each numerical model was categorized as bulging, splitting, or perforation and included in Table 3.

Table 3 Comparison of experimental results with numerical analyses results

Test No.	Test Specimen	Experimental Results				Numerical Analyses Results					
		Test Result	Damage mode	Penetration Depth	Bulging Depth	FEA Result	Damage mode	Penetration Depth		Bulging Depth	
				x_{c_test} (in)	x_{bg_test} (in)			x_{c_FEM} (in)	x_{c_FEM}/x_{c_test}	x_{bg_FEM} (in)	x_{bg_FEM}/x_{bg_test}
1	3.7-0.37-50-1.0-1.3-554	Stopped	Bulging	2.06	0.25	Stopped	Bulging	2.25	1.09	0.31	1.25
2	3.7-0.37-50-1.0-1.3-677	Stopped	Bulging	3.06	0.63	Stopped	Bulging	2.77	0.91	0.41	0.66
3	3.7-0.37-50-1.0-2.0-430	Stopped	Bulging	1.56	0.25	Stopped	Bulging	1.99	1.28	0.21	0.85
4	3.7-0.37-50-1.0-2.0-525	Stopped	Bulging	3.16	0.58	Stopped	Bulging	3.18	1.01	0.44	0.76
5	3.7-0.53-50-1.5-1.3-660	Stopped	Bulging	1.38	0.56	Stopped	Bulging	1.19	0.86	0.49	0.87
6	3.7-0.53-50-1.5-1.3-750	Stopped	Bulging	2.00	0.72	Stopped	Bulging	2.08	1.04	0.53	0.74
7	3.7-0.53-50-1.0-2.0-513	Perforated	Perforation	-	-	Perforated	Perforation	-	-	-	-
8	3.7-0.53-50-1.0-2.0-626	Perforated	Perforation	-	-	Perforated	Perforation	-	-	-	-
9	3.7-1.23-50-1.5-3.5-380	Stopped	Splitting	4.00	1.63	Perforated	Perforation	-	-	-	-
10	3.7-1.23-50-1.5-3.5-465	Stopped	Bulging	1.91	0.59	Perforated	Perforation	-	-	-	-

In all but two test cases (number 9 and 10), the numerical models resulted in the same damage modes as the experimental test results. The estimation of penetration depth and bulging depth showed good agreement with the test results. Based on the data in Table 3, the penetration depth was estimated with an average of 3% error and standard deviation of 13%. For bulging depth, the estimation from the numerical models had an average of 14% error and standard deviation of 19%, when compared to the experimental results. This statistical comparison is summarized in Table 4

Table 4 Statistical evaluation of benchmarking results

	Penetration x_{c_FEM}/x_{c_test}	***Bulging*** x_{bg_FEM}/x_{bg_test}
μ	1.03	0.86
σ	0.13	0.19
COV	0.13	0.22

Observation of the rear steel faceplate rupture of SC wall specimen provides a qualitative comparison of the numerical model to experimental results. For the splitting case which occurred on the rear faceplate in test number 9, the rupture initiated at a tie bar hole and propagated horizontally to the next tie bar hole. The rupture propagated one full spacing to the left and one-half spacing to the right with a small amount of vertical rupture downward. Seven of the ends of the tie bars, around the center of the rear steel faceplate, were found to be broken and popped off the specimen as can be seen in Figure 5 (a). Even if the numerical analysis of this test case resulted in perforation damage mode, it is close to the splitting damage mode which precedes perforation. The shape of the ruptured steel faceplate agreed reasonably with the experimental test results as illustrated in Figure 5 (b).

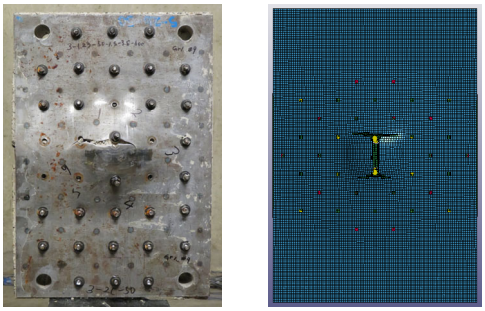

(a) Test result (b) Numerical analysis result

Figure 5 Splitting damage mode in experimental test and numerical analysis (#9) (Kim et al., 2021, 2022)

Test numbers 7 and 8 produced perforation damage mode and the result of the former case was photographed as a representative perforation (see Figure 6 (a)). The perforation occurred in the exact center of the rear steel faceplate with resultant tearing in four directions forming a cross shape. Figure 6 (b) shows the numerical analysis result which compared well with the test result. Examination of the numerical simulation revealed that splitting occurred, generating a cross shape of rupture. As the projectile continued moving forward, the cross shape of rupture increased and opened enough for the projectile to pass through. A couple of tie bar ends around the center of the rear steel faceplate were broken and their heads were popped off in the experimental result. Figure 7 (a) shows contour plots of the maximum principal strains through the central cross section of the numerical model. Figure 7 (b) illustrates cross section cut of the experimental test specimen. The failure mechanism of the SC wall was verified including formation of the concrete plug and rupture of the rear steel faceplate.

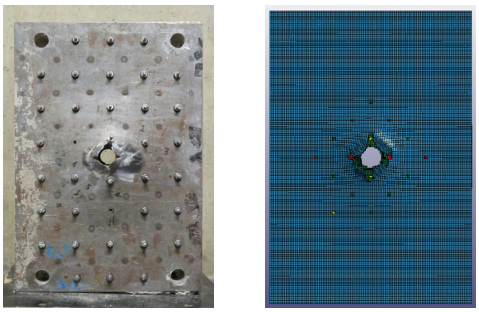

(a) Test result (b) Numerical analysis result

Figure 6 Perforation failure in experimental test and numerical analysis (#7) (Kim et al. 2021, 2022)

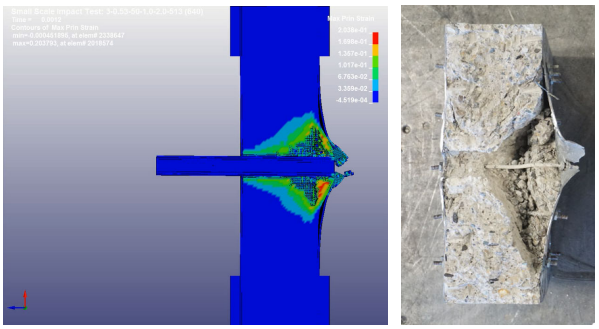

(a) Max. principal strains contour plots (b) Cross section cut of the specimen

Figure 7 Contour plots of the maximum principal strains through cross section (#7) (Kim et al., 2021, 2022)

4. SUMMARY AND CONCLUSIONS

All the specimens in this test program were small-scale SC walls and designed referring to AISC N690s1-15, Appendix N9. Experimental tests verified that projectiles flew straight without pitching and yawing, and struck the exact center of the specimens as intended. Chambers in the test setup confined all the debris from the projectiles and specimens effectively and safely. Results of ten experimental test cases were presented from the SC wall specimens with varied cross sectional configuration subjected to impact from a variety of projectiles. Post-tested SC wall specimens were examined carefully and three different types of damage mode such as bulging, splitting and perforation were observed. Consequently, the experimental methodology including SC wall specimen design, test setup, and instrumentation was proven to be appropriate for this projectile impact test research.

Three-dimensional finite element models were developed to simulate the small-scale missile impact test and the benchmarked with the experimental test results. Perforation check, penetration depth and bulging depth were compared between finite element analyses and experimental tests. Eight out of ten simulation cases resulted in the same result (stopped or perforated) and the other two simulation cases provided conservative results. Simulations estimated penetration depth and bulging depth accurately. Additionally, rupture shape of the rear steel faceplate was compared between numerical simulation and experimental tests. When the SC wall specimen had splitting or perforation damage mode, the rupture shape of the rear faceplate leading to its final stage of failure agreed. Therefore, the benchmarking results confirmed the validity of the numerical approach presented herein.

As future work, the experimental investigation will continue and be used to refine the design method included in the commentary of AISC N690s1-15,

Appendix N9. The numerical modeling approach will also be applied to larger-scale SC wall specimens subjected to missile impact to evaluate its validity and accuracy for estimating local failure behavior of larger specimens.

ACKNOWLEDGEMENTS

The research presented in this paper was funded by United States Nuclear Regulatory Commission (USNRC) and Korea Hydro and Nuclear Power (KHNP).

REFERENCES

AISC. (2015). *Specification for Safety-Related Steel Structures for Nuclear Facilities Including Supplement No. 1 (ANSI/AISC N690s1-15)*. American Institute of Steel Construction.

Bruhl, J. C., Varma, A. H., and Johnson, W. H. (2015). "Design of composite SC walls to prevent perforation from missile impact." *International Journal of Impact Engineering*, Elsevier Ltd, 75, 75–87.

Kim, J. M., Bruhl, J., Seo, J., and Varma, A. (2017a). "An overview of missile impact tests on Steel-plate Composite (SC) walls." *Structures Congress 2017: Blast, Impact Loading and Response of Structures - Selected Papers from the Structures Congress 2017*.

Kim, J. M., Varma, A., Lee, K., and Kim, K. (2022). "Steel-Plate Composite Walls Subjected to Missile Impact: Numerical Evaluation of Local Damage." *Journal of Structural Engineering*, 148(10).

Kim, J. M., Varma, A., Seo, J., Bruhl, J., Lee, K., and Kim, K. (2017b). "Resistance of SC Walls Subjected to Missile Impact: Part 3. Small-Scale Tests." *Transactions of the 24th International Conference of Structural Mechanics in Reactor Technology (SMiRT-24)*, Busan, South Korea.

Kim, J. M., Varma, A., Seo, J., Bruhl, J., Lee, K., and Kim, K. (2021). "Steel-Plate Composite Walls Subjected to Missile Impact: Experimental Evaluation of Local Damage." *Journal of Structural Engineering*, 147(2).

U.S. Department of Defense. (2008). "Unified Facilities Criteria (UFC) Structures to Resist the Effects of Accidental Explosions."